Electronic supplementary materials *Mendeleev Commun.*, 2021, **31**, 465–468

Effect of heterovalent doping on photostimulated defect formation in $CsPbBr_3$

Ibrahim M. Sharaf, Anna V. Shurukhina, Irina S. Komarova and Alexei V. Emeline

Photoresistant and photosensitive solids.

In general, there are two major mechanisms of photoinduced defect formation characterizing whether the solid material is photoresistant or photosensitive[21, 22]. The first mechanism is typical for the photoresistant solids and can be describe as following:

1. $D + e(h, e^0) \rightarrow D^{-(+)}$ (S1)

2. $D^{-(+)} + h(e, e^0) \rightarrow D$ (S2)

Here D is a preexisting defect state, $D^{-(+)}$ is a defect state with trapped charge carrier of the certain charge sign, and e, h, e^0 denote electrons, holes and excitons, respectively. Accordingly, equation 1 describes a charge carrier trapping by or exciton decay at preexisting defect states, D, resulting in formation of the new defect states $D^{-(+)}$, that depends on the type of original defect states and a sign of the trapped charge carrier, and equation 2 reflects a recombination process with charge carrier or exciton restoring the original state of the defects. It is easy to demonstrate that kinetics of photoinduced formation of defects, $D^{-(+)}$, obeys an exponential dependence[23]:

$$D^{-(+)}_{(t)} = D_o \frac{p}{p+q}\left(1 - e^{-(p+q)t}\right) \quad \text{(S3)}$$

which is characterized by saturation limit achieved at stationary irradiation:

$$D^{-(+)}_{\infty} = D_o \frac{p}{p+q} \quad \text{(S4)}$$

Here D_0 is an initial concentration of the preexisting defects, D, and *p* and *q* are the probabilities of the formation and decay of photoinduced defect states, $D^{-(+)}$, in accordance with equations 1 and 2. Thus, the total number of the defect states remains the same during photoexcitation, and therefore, the solids demonstrating such behavior are photoresistant. For example, this type of the photoinduced defect formation is typical for most metal oxides.

In opposite, photosensitive solids are characterized by formation of new defects as a result of electronic excitation energy dissipation in the crystal lattice. A typical mechanism of defect formation is associated with the exciton decay on the regular lattice sites:

$L + e^0 \rightarrow D' + D''$ (S5)

Here L denotes a regular lattice sites and D’ and D’’ a pair of new formed defect states, such as Frenkel defect pair. These defects are formed as a result of the ion displacement from the regular site to interstitial position due to energy of exciton localized at the regular site. The necessary conditions for the realization of this mechanism are:

1) a possibility of exciton self-trapping at the regular site (that provides a condition for the localization of excitation),

2) a life time of self-trapped exciton must be longer than a period of the lattice vibrations (that provides a condition for the exciton energy release during atomic vibration in the lattice),

3) an energy of exciton must be higher than an energy required for the defect formation (that provides an energy required for the defect formation).

This conditions for the photoinduced defect formation are typically satisfied in such photosensitive solids such as metal halides. Consequently, this type of defect formation can be expected in halide perovskites as well.

As following from the equation 5 kinetics of defect formation linearly depends on the light exposition (either on time of irradiation or on light intensity) at least at the initial period of irradiation when the density of the regular sites is much higher than a density of the defects in solids. That is:

$$D'_t(D''_t) = p\ I\ t \qquad (S6)$$

here p is a probability of the defect formation, I is a light intensity, and t is a time of irradiation.

Thus, in the simplified case a difference between two mechanisms, and therefore, between photoresistant and photosensitive character of perovskites, can be distinguished by kinetics of photoinduced defect formation: exponential *vs*. linear.

Synthesis

Both Ag-doped and Bi-doped $CsPbBr_3$ microdispersed samples as well as an undoped $CsPbBr_3$ reference sample were synthesized via the chemical precipitation method. CsBr (98%, ZRM), $PbBr_2$ (98% Sigma-Aldrich) and HBr (56%, Lenreactiv) were used as received without further purification. $BiBr_3$ and AgBr were obtained and purified in the laboratory from the corresponding metal nitrates with HBr.

For synthesis of $CsPbBr_3$ perovskite powder, 2 mmol $PbBr_2$ with 1 mmol CsBr were dissolved separately in 10 ml HBr. Then, $PbBr_2$ solution was added dropwise with vigorous stirring to the clear solution of CsBr. 5% excess of lead bromide solution was added into resulting solution to suppress a formation of the Cs_2PbBr_6 phase. The solution was heated at 280ºC until the powder appears. Then, the resulting precipitate was collected using a Schott filter. The residue was washed with the small amount of HBr and the unreacted agent was removed. Finally, the

sediment was dried under vacuum conditions overnight to obtain an orange $CsPbBr_3$ powder. Synthesis of the doped samples was performed in a similar way. Before the synthesis procedure, a required amount of either AgBr or $BiBr_3$ was added to the solution containing $PbBr_2$ and stirred until complete dissolution.

XRD

Crystal phase determination was performed by X-ray diffraction method with a Rigaku Miniflex II diffractometer with CuKα radiation in the range of angles of $10° \leq 2\theta \leq 60°$ with a scanning speed of 5.0° / min. Corresponding diffractograms are presented in Figure S1 and confirm a successful formation of $CsPbBr_3$ orthorhombic perovskite phase for both doped and undoped samples.

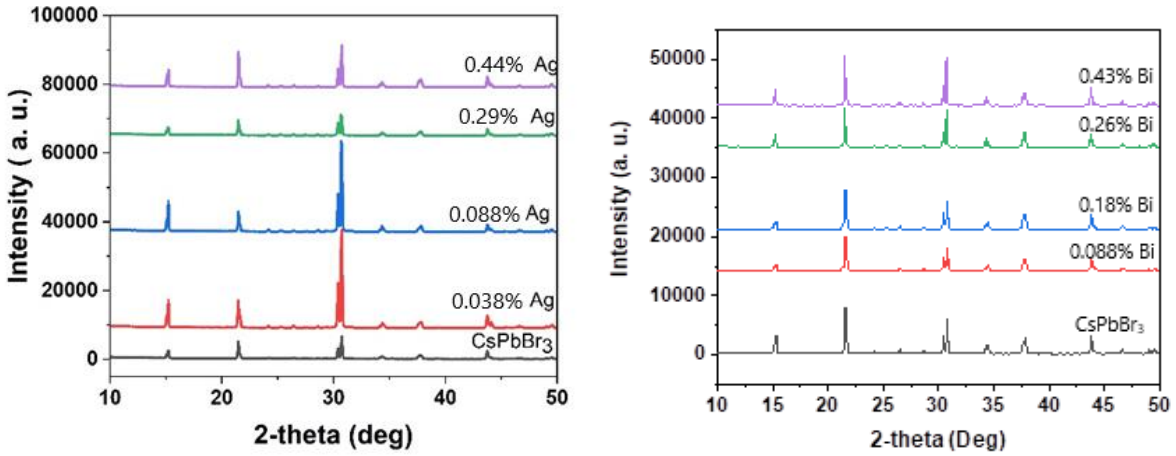

a) b)

Figure S1. (a) X-ray diffraction patterns of Ag-doped (a) and Bi-doped (b) $CsPbBr_3$ samples.

The XRD patterns of the as-synthesized doped and undoped $CsPbBr_3$ samples are single-phase and no any other impurities distinct diffraction peaks apart the $CsPbBr_3$ orthorhombic phase have been found. All $CsPbBr_3$ perovskite samples demonstrate XRD diffraction peaks at 15.2°, 21.5°, 30.7°, 37.7°, and 43.8° corresponding to (110), (112), (220), (024), and (224) planes with lattice indices a = 8.21 Å, b = 8.25 Å, and c = 11.76 Å, with space group Pbnm [22].

SEM

The perovskite microcrystal morphology observation was performed using a Hitachi S-3400N scanning electron microscope. The corresponding images of the doped and undoped samples are shown in Figure S2. They demonstrate a formation of micro-size particles of $CsPbBr_3$.

a)

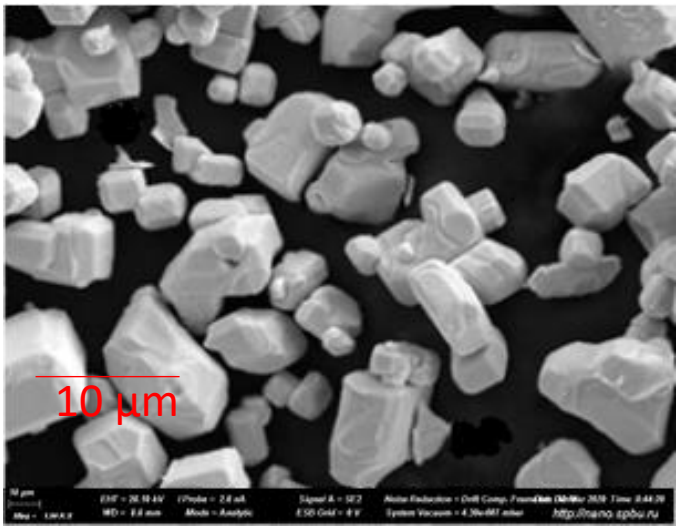

b)

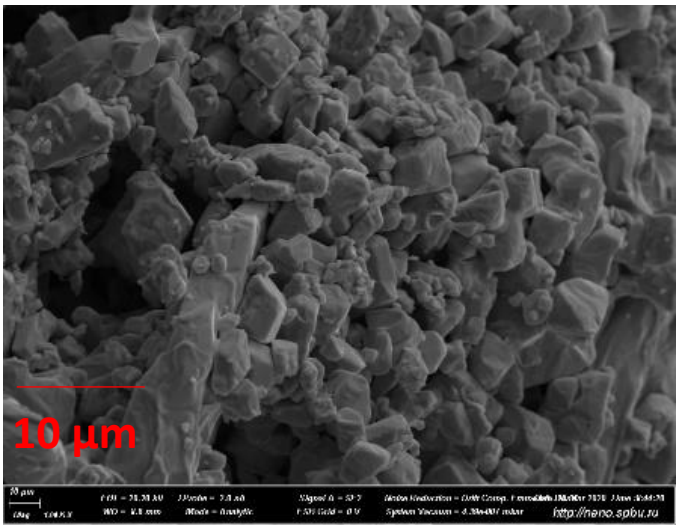

c)

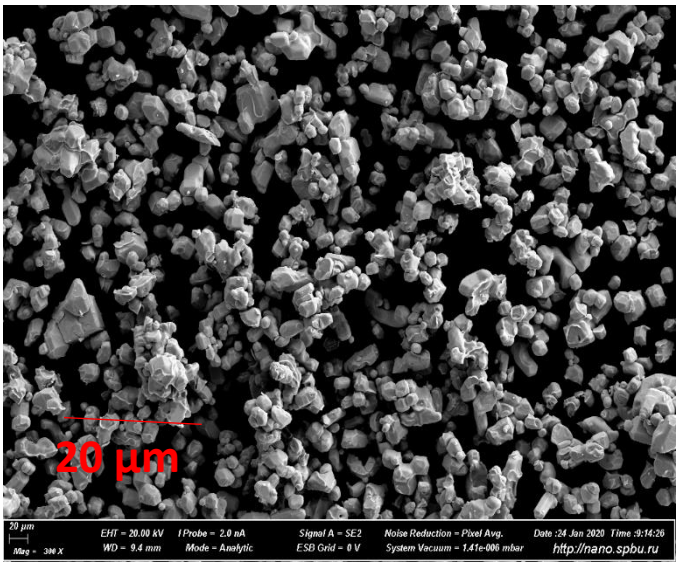

Figure S2. SEM images of pristine (a), Bi(0,43 at%) doped (b), and Ag(0,44 at%) doped (c) $CsPbBr_3$.

XPS

The chemical composition of $CsPbBr_3$ perovskites was studied using X-ray photoelectron spectroscopy (XPS), as presented in Figures S2 and S3. The XPS spectra (see Figures S3 and S4) were collected using Thermo Fisher Scientific ESCALAB 250Xi setup with Al-Kα X-ray source (1486.6 eV with monochromator), variable beam size (200-900 mkm) and energy resolution 0.45 eV. The signal binding energies correspond to the Cs, Pb, Br for all samples and to both Ag and Bi for the corresponding doped $CsPbBr_3$. These results demonstrated the presence of Ag and Bi ions within the perovskite structures and enhanced intensities with increased concentrations of dopants indicating the effectiveness of the doping process.

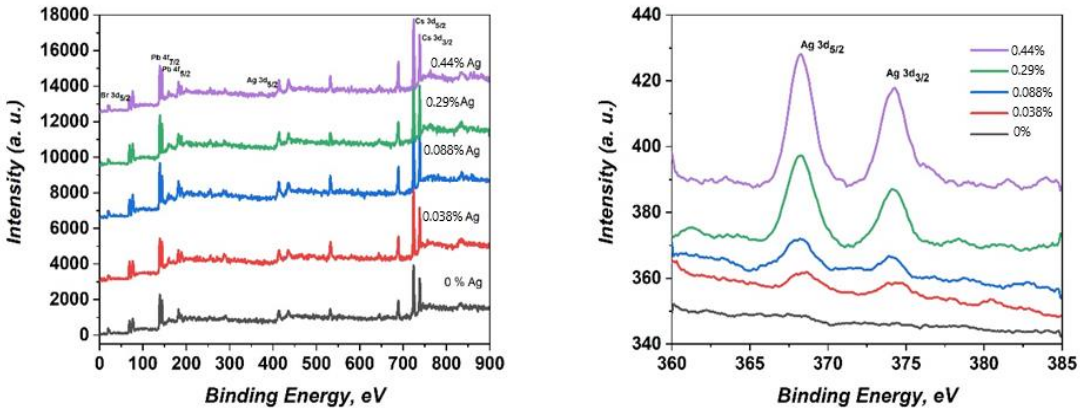

a) b)

Figure S3. a) XPS spectra of Ag-doped $CsPbBr_3$: a) survey spectra, and b) Ag 3d XPS spectra.

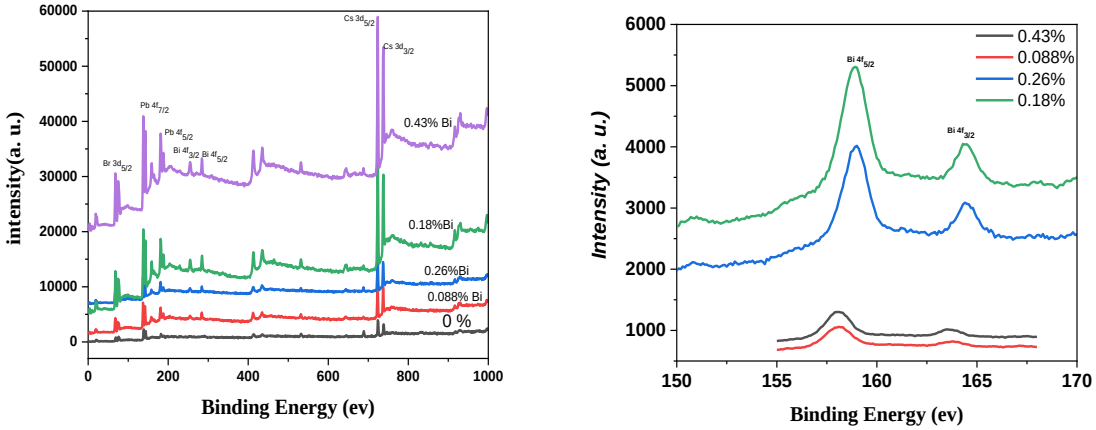

a) b)

Figure S4. a) XPS spectra of Bi-doped $CsPbBr_3$: a) survey spectra, and b) Bi 4f XPS spectra.

Photostimulated defect formation

Irradiation of the samples during experiments on photostimulated defect formation was performed with Hg-lamp DRK-120 (LOMO) equipped with an interference band-pass filter selecting 436 nm mercury line. Intensity of irradiation was 11±1 μW cm^{-2}.

Diffuse reflection spectra (DRS) R (λ) were recorded in the spectral range of 436-800 nm at room temperature using a Cary 5000 spectrophotometer equipped with an external diffuse reflection sphere DRS 2500. The optical-class Spectralon was used as a reference sample.

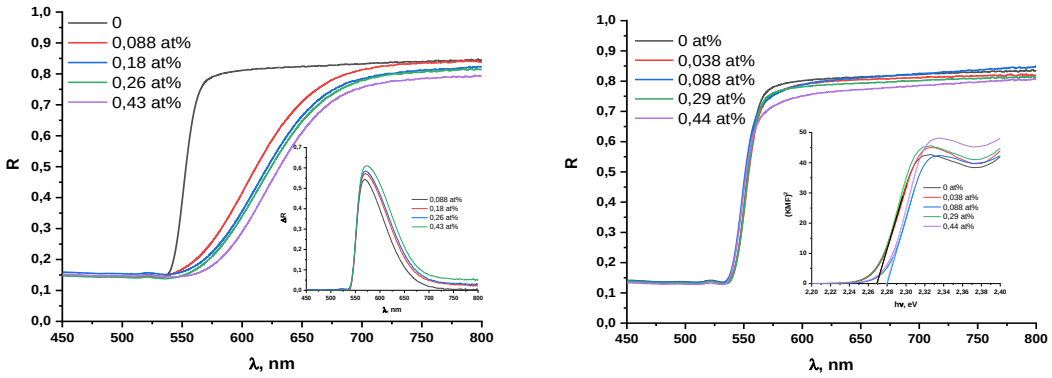

a) b)

Figure S5. Diffuse reflectance spectra of the set of Bi-doped (a), and Ag-doped $CsPbBr_3$. Inset in Figure 1(a) demonstrates a difference spectrum between DRS of pristine and Bi-doped samples. Inset in Figure 1(b) demonstrates replotting of Kubelka-Munk function to determine band gap values of the Ag-doped samples.

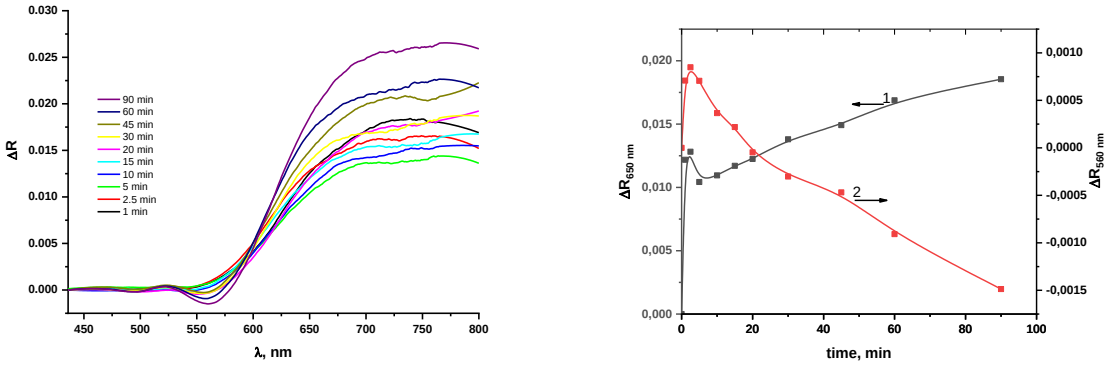

a) b)

Figure S6. Time evolution of the defect absorption in Bi(0,088 at%) doped $CsPbBr_3$ caused by irradiation at λ=436 nm: a) difference diffuse reflectance spectra at different irradiation time; b) kinetics of diffuse reflectance alteration recorded for wavelengths 650 nm (1) and 560 nm (2).

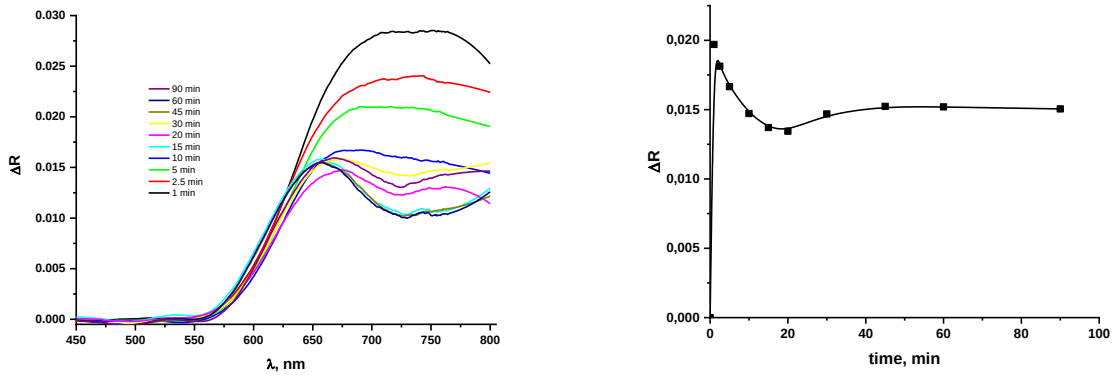

a) b)

Figure S7. Time evolution of the defect absorption in Bi(0,18 at%) doped $CsPbBr_3$ caused by irradiation at λ=436 nm: a) difference diffuse reflectance spectra at different irradiation time; b) kinetics of diffuse reflectance alteration recorded for wavelength 650 nm.

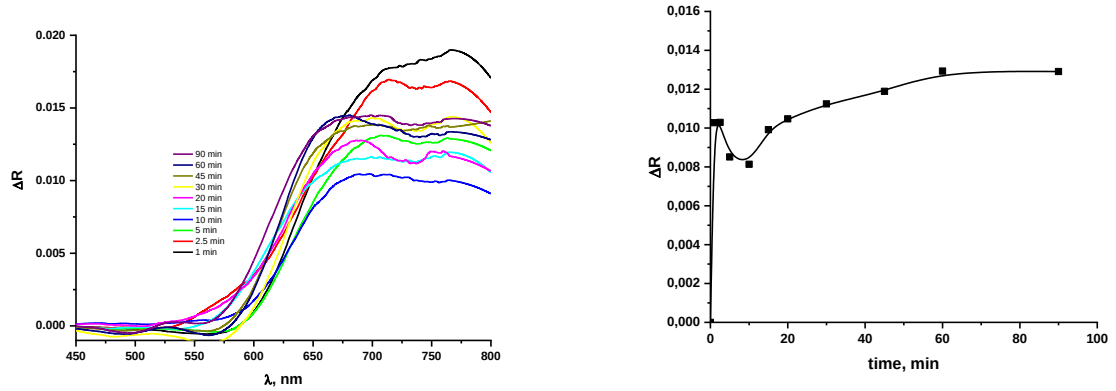

a) b)

Figure S8. Time evolution of the defect absorption in Bi(0,26 at%) doped $CsPbBr_3$ caused by irradiation at λ=436 nm: a) difference diffuse reflectance spectra at different irradiation time; b) kinetics of diffuse reflectance alteration recorded for wavelength 650 nm.

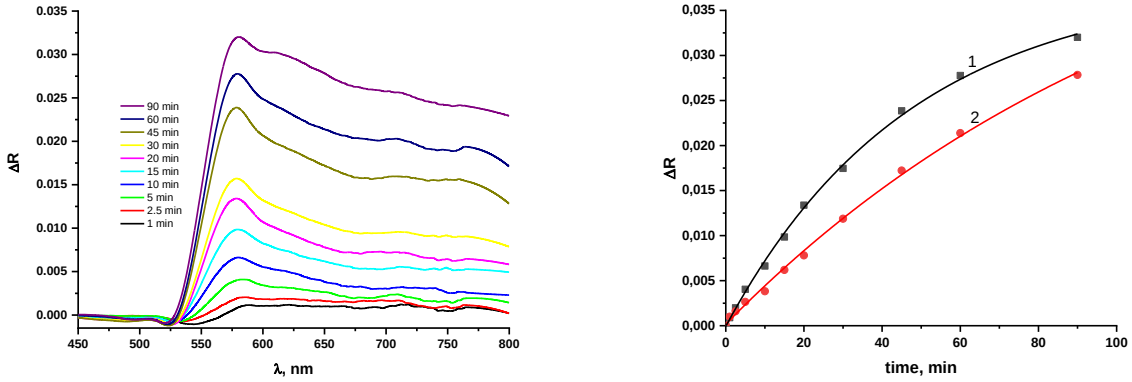

a) b)

Figure S9. Time evolution of the defect absorption in Ag(0,038 at.%) doped $CsPbBr_3$ caused by irradiation at λ=436 nm: a) difference diffuse reflectance spectra at different irradiation time; b) kinetics of diffuse reflectance alteration recorded for wavelengths 580 nm (1) and 650 nm (2).

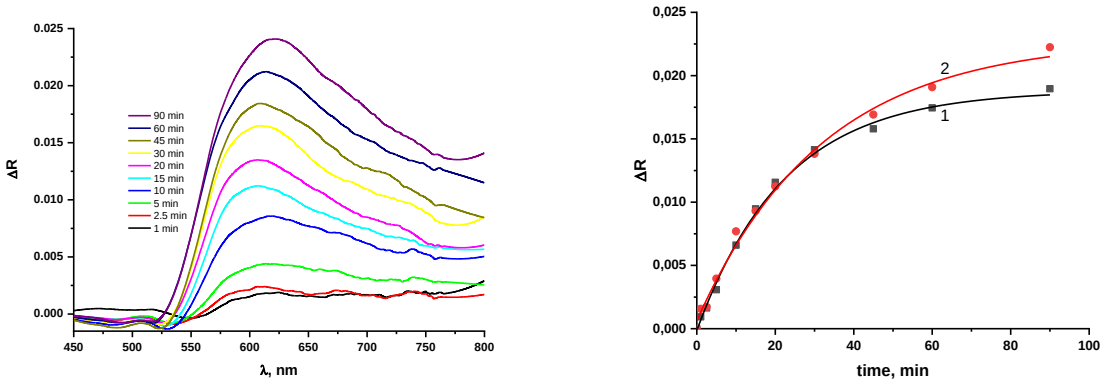

a) b)

Figure S10. Time evolution of the defect absorption in Ag(0,088 at.%) doped $CsPbBr_3$ caused by irradiation at λ=436 nm: a) difference diffuse reflectance spectra at different irradiation time; b) kinetics of diffuse reflectance alteration recorded for wavelengths 580 nm (1) and 650 nm (2).

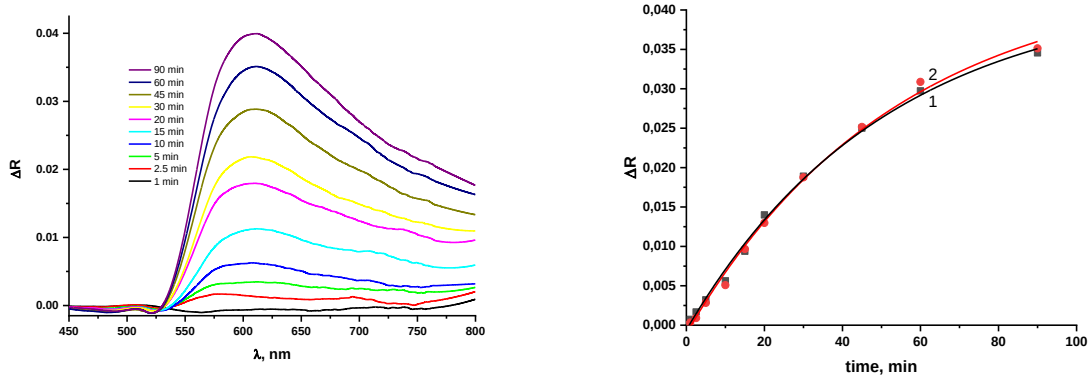

a) b)

Figure S11. Time evolution of the defect absorption in Ag(0,29 at.%) doped $CsPbBr_3$ caused by irradiation at λ=436 nm: a) difference diffuse reflectance spectra at different irradiation time; b) kinetics of diffuse reflectance alteration recorded for wavelengths 580 nm (1) and 650 nm (2).